J Ther Eng, Vol. 9, No. 5, pp. 1667−1686, September, 2023

Journal of Thermal Engineering
Web page info: https://jten.yildiz.edu.tr
DOI: 10.18186/thermal.1401685

Research Article

Flow field and heat transfer of ferromagnetic nanofluid in presence of magnetic field inside a corrugated tube

Aram Soleimani VARKANEH[1], Ghanbar Ali SHEIKHZADEH NOOSHABADI[2], Ali Akbar ABBASIAN ARANI[3,*]

[1]*Department of Mechanics, Energy Conversion, Islamic Azad University, Arak Branch, Arak, 3836119131, Iran*
[2]*Department of Mechanical Engineering, Heat and Fluid, University of Kashan, Kashan, Iran, and Islamic Azad University, Arak Branch, Arak, 3836119131, Iran*
[3]*Department of Mechanical Engineering, Heat and Fluid, University of Kashan, Kashan, Iran, and Islamic Azad University, Arak Branch, Arak, 3836119131, Iran*

ARTICLE INFO

Article history
Received: 30 July 2021
Accepted: 24 November 2022

Keywords:
Heat exchanger; Helical ribs; Nanofluid; Two-phase mixture model; Magnetic field; Corrugation

ABSTRACT

The present study investigates the effects of using a magnetic field on the flow field and heat transfer of ferromagnetic Fe_3O_4/H_2O nanofluid considering two-phase model for nanofluid in heat exchanger equipped with helical ribs. Three methods are employed to enhance the thermal efficiency of heat exchanger, as employing of corrugations, utilizing nanofluid as heat transfer fluid, and employing the magnetic field. The performance evaluation criteria index (PEC) is employed to analyze the thermal-hydraulic characteristics of the heat exchanger. The main aim is to achieve an optimum model with the highest performance evaluation criteria value. Usaging of corrugated heat exchanger or nanofluid can increase the average Nusselt number and friction factor in the tube sharply. Also, it is understood that the presence of a magnetic field has a significant effect on the heat transfer enhancement inside the heat exchanger. The model with magnetic field of 600 G has the highest Nusselt number ratio among all studied models, which is followed with 400 G, 200 G, and 0 magnetic fields, respectively. Furthermore the effects of different corrugation heights, widths, and pitches have been studied. Finally, usage of the novel corrugated heat exchanger with 14 mm corrugation heights, 9 mm rib width, and 12.5 mm blade pitches filled with nanofluid, and under a magnetic field of 600 G it suggested as the most efficient configuration. Also, at the Reynolds number of 4,000, the highest performance evaluation criteria values are achieved.

Cite this article as: Varkaneh AS, Sheikhzadeh Nooshabadi GA, Abbasian Arani AA. Flow field and heat transfer of ferromagnetic nanofluid in presence of magnetic field inside a corrugated tube. J Ther Eng 2023;9(5):1667−1686.

***Corresponding author.**
*E-mail address: abbasian@kashanu.ac.ir

This paper was recommended for publication in revised form by Regional Editor Emre Alpman

Published by Yıldız Technical University Press, İstanbul, Turkey

INTRODUCTION

The investigation of heat transfer and boundary layer flows due to utilizing corrugated channels or ribbed tubes and also employing inserting obstacles has become more and more important in many engineering processes with industrial applications such as heat exchangers [1], electronic cooling devices [2], thermal regenerators [3], automobile engine cooling [4], solar heating [5] and air conditioning systems [6]. This is the reason that convective heat transfer and fluid flows through tubes containing corrugations are investigated by numerous researchers [7-13]. Moreover, because of the rising requirement for the developments of heat transfer and fluids flow with better thermal characteristics than common fluids, the nanofluid investigations in thermal systems are more and more significant [14-21].

The word nanofluid refers to an especial class of heat fluids, which includes solid particles in nano range of 1 to 100 nm homogeneously dispersed in a common base fluid such as thermal-oil, ethylene glycol or water. Nanoparticles can be metallic solids (such as Al, Ag, and Cu) or nonmetallic solids (such as Fe_2O_3, CuO, and Al_2O_3) [22-26]. The addition of metal or metal oxide nanoparticles to a common base fluid increases the thermal conductivity coefficient of the final fluid. In other words, nanofluid is a well-versed heat transfer or coolant fluid which has gained a considerable acknowledgment in different thermal requests and applications. Additionally, nanofluid offers increased thermal conductivity coefficient, which can improve the efficiency of thermal systems without an important upsurge in pressure drop. This will finally decrease the size and dimensions of thermal systems and, therefore, the costs of production [27].

The electric field can be mentioned as one of the effective active techniques for improving heat transfer [28]. This method can be combined with another passive way, namely nanofluid. The examinations of Magneto-Hydro-Dynamic (MHD) flows are so important in industries and have continued requests in different research areas such as metallurgical processes and petroleum productions [29]. MHD is the science of investigating electrically conducting fluid flows in the presence of an external magnetic field, and it has gained considerable attention of researchers because of its protruding role in different thermal systems and engineering processes such as the fluid flows in microelectronic systems, the flow of liquid metals and crystal growth [30, 31].

Zainala et al. [26] studied numerically and employing MATLAB software for the MHD mixed convection heat transfer in a vertical flat plate heat exchanger filled with single-phase water-based Cu-Al_2O_3 hybrid nanofluid. According to their obtained results, the nanofluid velocity and temperature upsurges and reduced respectively with an increase of magnetic field parameter. Job and Gunakala [27] studied numerically MHD fluid flow and heat transfer inside two elastic coaxial pipes pulsatile equipped with porous blocks and filled with water-based CuO nanofluid. He understood that thermal efficiency improves with the increase of solid nanoparticles diameter and volume concentration, Reynolds number, and the elastic modulus of the pipes. Daneshvar Garmroodi et al. [28] studied numerically laminar MHD mixed convection of a cavity equipped with two multiple rotating cylinders and filled with two-phase water-based Cu nanofluid. They found that thermal efficiency reduces by an increase of Hartmann number.

Eid [29] studied numerically effects of chemical reactions on MHD free convection heat transfer inside an exponentially stretching sheet equipped with heat sources and filled with two-phase nanofluid. He reported interesting results such as, skin friction coefficient, Sherwood number, average Nusselt number, dimensionless velocity, dimensionless temperature, and concentration contours of nanoparticles. Ma et al. [30] investigated numerically laminar MHD convective heat transfer in a two dimensional corrugated channel with active heaters and coolers and filled with water-based Ag-MgO hybrid nanofluid. They realized that the highest Nusselt number occurs at the heater junction and the cooler junction. Sheikholeslami and Rokni [31] studied numerically MHD nanofluid flow in the presence of Lorentz forces. They found that the Nusselt number surges by Hartmann number increase, and the temperature gradients reduce by increasing the Eckert number and melting parameter. Jafarimoghaddam [32] studied numerically MHD porous flow of a three-dimensional bidirectional stretching surface filled with two-phase Upper-Convected-Maxwell (UCM) nanofluid. Eid and Mahny [33] studied numerically unsteady MHD heat and mass transfer and fluid flow over a permeable stretching wall with heat generation/absorption and filled with non-Newtonian two-phase nanofluid. It is found that the concentration and thermal boundary-layer thickness values increase by the increase of the magnetic field. In a reviewed paper by Sajid [34], they show the effects of concentration of nanoparticles and nanofluid flow rate on pressure drop, friction factor, and Nusselt number from several investigations. Kumar [35] investigated experimentally PEC of a minichannel filled with Al_2O_3/MWCNT hybrid nanofluid. Izadi et al. [36] present a numerical investigation on laminar MHD heat transfer and fluid flow in the cooling process inside a porous metal CPU system, which is filled with nanofluid. They understood that usage of a magnetic field with a stronger filed or system with higher porous metal foam can improve the impingement cooling heat transfer.

Sheikholeslami [37] studied numerically effects of Brownian motions and nanoparticle shapes on fluid flow and heat transfer in a porous media filled with water-based CuO nanofluid in the presence of a magnetic field. He found that convective heat transfer improves with augmentation of Darcy and Reynolds number, but it reduces with the rise of Hartmann number. Elahi et al. [38] investigated mathematically on the heat transfer characteristics inside a channels. The results display a good idea based on the various methods in channels in order to optimize the thermal characteristics.

Selimefendigil and Oztop [39] investigated numerically MHD pulsating forced convective heat transfer over two parallel plates equipped with a blocks in channel, and filled with nanofluid. They found that the heat transfer of nanofluid at highest particle volume fraction are higher in pulsating flow as compared to base fluid and they are slightly different than the ones obtained in the steady flow. For more results in this filed one can refer to the exist investigation in literature [40-43].The literature review indicates that the effects of magnetic field on the flow field and heat transfer of ferromagnetic nanofluid with consideration of a two-phase model for nanofluid in a heat exchanger equipped with helical ribs is not studied by researchers. In the present study, three methods are employed to enhance the thermal efficiency of heat exchanger (HE):

- Usage of corrugations
- Utilizing of nanofluid as Heat Transfer Fluid (HTF)
- Using of a magnetic field

Different magnetic fields intensities and geometrical parameters are studied in this paper. But employing of corrugations and nanofluid can also increase the pressure drop penalty in heat exchanger. Therefore the Performance Evaluation Criteria (PEC) index is employed in the present investigation to analyze the thermal-hydraulic characteristics of heat exchanger. The main aim of the current paper is to achieve an optimum model with the highest PEC value.

NUMERICAL MODEL

Physical Model

The present paper investigates effects of employing a magnetic field on the flow field and heat transfer of ferromagnetic nanofluid with consideration of a two-phase model for nanofluid in a helix-corrugated heat exchanger. Fig. 1 illustrates the schematic diagram of configuration and geometrical parameters of the studied corrugated tube filled with HTF and under constant heat flux and magnetic field. The length of HE is 200.0 mm, and the tube diameter is 50.0 mm. Also, the inlet length of 830.0 mm and outlet length of 66.0 mm are determined because it is important that the inlet flow must be fully developed, and there not be any flow comeback at the exit section of the channel [1, 44]. The HE is made of stainless steel 304 with 2.0 mm thickness. The velocity inlet boundary condition is applied in the entrance of the inlet section with the certain temperature (T_{in}) and velocity (u_{in}), and the pressure outlet boundary condition has been adopted in the output of the exit section with zero gage pressure. Also, five different Reynolds numbers in the range of 4,000 to 20,000 are studied. These investigated Reynolds numbers are in the turbulent flow regime.

For all the investigated models, the initial nanofluid temperature is T_{in}=300K, and the constant heat flux of q=70,000 W/m^2 is adopted. Besides, four different constant magnetic fields (B= 0, 200, 400, and 600 G) are determined to analyze the effects of employing MHD fluid flow in HE under a magnetic field. The HTF is Fe_3O_4/H_2O nanofluid at nanoparticles volume fraction of ϕ = 1.0% and diameter of d_{np} = 20 nm. Table 1 reports geometrical parameters of studied HE. In the current study, effects of changing three geometrical parameters are analyzed, such as corrugation height, width, and pitch. Three different corrugation height values (b = 6.0, 10.0, and 14.0), three different corrugation width values (r=5.0, 9.0, and 13.0) and three different corrugation pitch values (p = 12.5, 20.0, and 27.5) are studied in this paper.

Governing Equations

The governing equations, including continuity, momentum, and energy equation for the nanofluid mixture, have been employed instead of employment of the governing equations of each solid- and fluid-phases separately [45]. The continuity:

$$\vec{\nabla}(\rho_m \vec{U}_m) = 0 \tag{1}$$

where the mass-averaged velocity ($\vec{U}_m$) has been calculated as [46]:

$$\vec{U}_m = \frac{\rho_s \phi_s \vec{U}_s + \rho_{bf} \phi_{bf} \vec{U}_{bf}}{\rho_m} \tag{2}$$

where $\vec{U}_s$ is the solid nanoparticles velocity, $\vec{U}_{bf}$ is the base fluid velocity, and ρ_m is the mixture density for the whole suspension and is written as [47]:

The momentum equation [47]:

$$\begin{aligned}\rho_m(\vec{U}_m \vec{\nabla} \vec{U}_m) &= -\vec{\nabla} p + \mu_m \left(\vec{\nabla} \vec{U}_m + (\vec{\nabla} \vec{U}_m)^T\right) \\ &+ \vec{\nabla}(\rho_{bf} \phi_{bf} \vec{U}_{dr,bf} \vec{U}_{dr,bf} + \rho_s \phi_s \vec{U}_{dr,s} \vec{U}_{dr,s}) + \rho_m g\end{aligned} \tag{3}$$

where μ_m is the mixture dynamic viscosity, p is pressure, $\vec{U}_{dr,bf}$ and $\vec{U}_{dr,s}$ are the drift velocity of solid phase and fluid phase [48]:

$$\vec{U}_{dr,bf} = \vec{U}_{bf} - \vec{U}_m \tag{4}$$

$$\vec{U}_{dr,s} = \vec{U}_s - \vec{U}_m \tag{5}$$

The energy equation is defined as follows [49]:

$$\vec{\nabla}(\rho_{bf} \phi_{bf} \vec{U}_{bf} h_{bf} + \rho_s \phi_s \vec{U}_s h_s) = \vec{\nabla}\left((\phi_{bf} k_{bf} + \phi_s k_s) \vec{\nabla} \mathrm{T}\right) \tag{6}$$

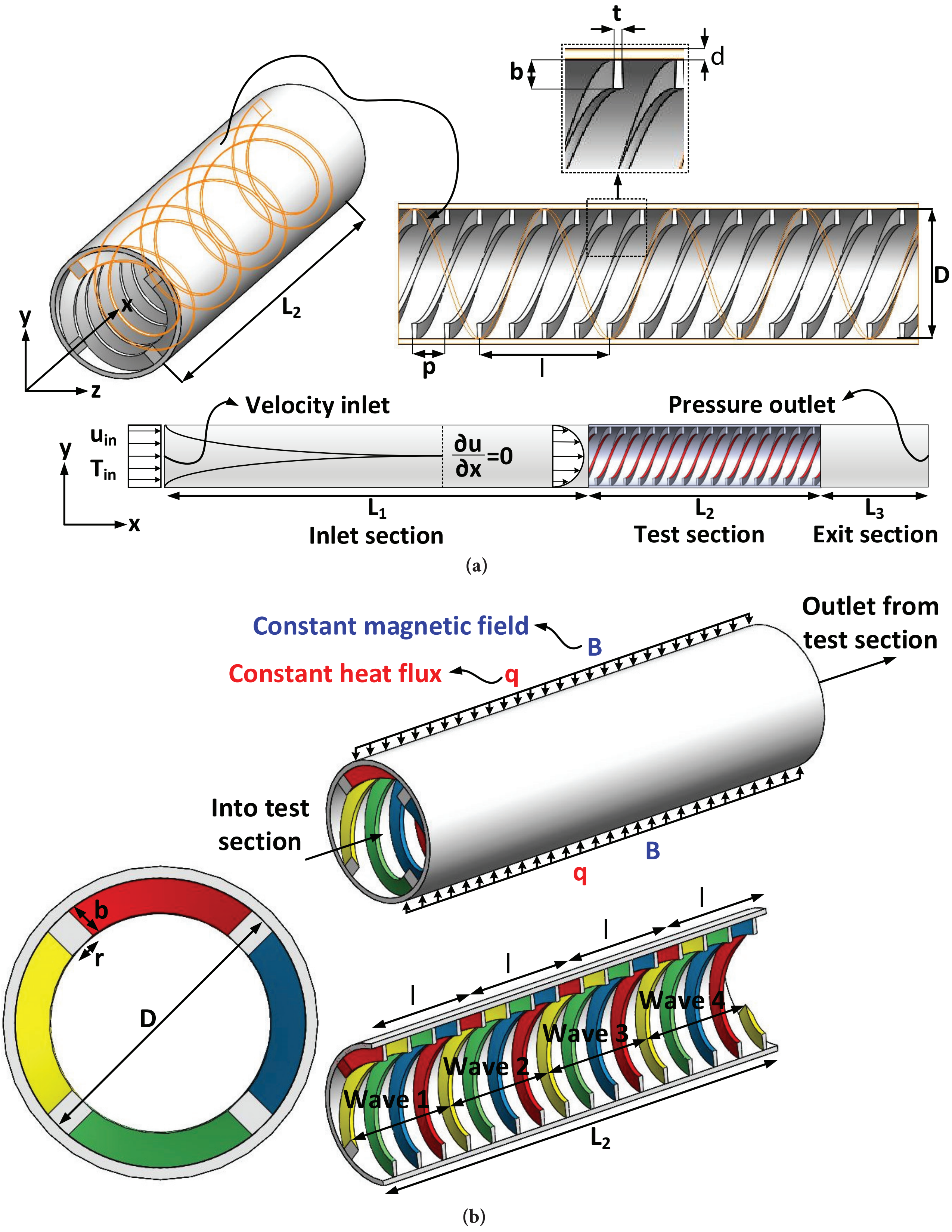

Figure 1. Schematic diagram of configuration and geometrical parameters of studied corrugated tube filled with HTF under constant heat flux and magnetic field.

Table 1. Geometrical parameters of studied HE

Parameter	Symbol (Unit) (mm)	Value
Inlet section length of HE	L_1	830.0
Test section length of HE	L_2	200.0
Exit section length of HE	L_3	66.0
Tube diameter	D	50.0
Tube thickness	δ	2.0
Corrugation height	b	6.0, 10.0 and 14.0
Corrugation width	r	5.0, 9.0 and 13.0
Corrugation thickness	t	2.0
Corrugations pitch	p	12.5, 20.0 and 27.5
Wavelength of helix	λ	50.5

where h_s and h_{bf} are the enthalpy of nanoparticles and base fluid, respectively. The nanoparticles volume concentration equation for suspension is as follows [50]:

$$\vec{\nabla}\left(\rho_s \phi_s \vec{U}_m\right) = -\vec{\nabla}\left(\rho_s \phi_s \vec{U}_{dr,s}\right) \tag{7}$$

The slip velocity is written as:

$$\vec{U}_{bf,s} = \vec{U}_{bf} - \vec{U}_s \tag{8}$$

where the relations between the relative and drift velocities are written as [47]:

$$\vec{U}_{dr,s} = \vec{U}_{s,bf} - \frac{\rho_s \phi_s}{\rho_m} \vec{U}_{bf,s} \tag{9}$$

The Schiller and Naumann [49] drag relative velocity is written as follow:

$$\vec{U}_{bf,s} = \frac{d_p^2}{18\mu_{bf} f_d} \frac{\rho_s - \rho_m}{\rho_s} \vec{\alpha} \tag{10}$$

$$f_d = 1 + 0.15\mathrm{Re}_s^{0.687} \tag{11}$$

$$\vec{\alpha} = \vec{g} - \left(\vec{U}_m \vec{\nabla} \vec{U}_m\right) \tag{12}$$

where, $\vec{\alpha}$ and $\vec{g}$ are the solid phase and base fluid gravity accelerations, respectively. The Reynolds of solid nanoparticles (Re_s) is calculated as [46]:

$$\mathrm{Re}_s = \frac{U_m d_p \rho_m}{\mu_m} \tag{13}$$

where d_p is the average diameter of solid nanoparticles and is assumed about 20 nm. The uniform magnetic field ($\vec{B} = B_x \vec{e_x} + B_y \vec{e_y}$) of constant magnitude $B = \sqrt{B_x^2 + B_y^2}$ is applied, where $\vec{e_x}$ and $\vec{e_y}$ are unit vectors. The orientation of the magnetic field forms an angle θ with the horizontal axis such that $\cot\theta = B_x/B_y$. The electromagnetic force $\vec{F}$ and the electric current $\vec{J}$ are defined by $\vec{F} = \sigma\left(\vec{V} \times \vec{B}\right) \times \vec{B}$ and $\vec{J} = \sigma(\vec{V} \times \vec{B})$, respectively. In current investigation, the magnetic field orientation is set to be horizontal (θ = 0)

Table 2. Most imortant non-dimensional number in MHD fluid flow [52-54]

Non- dimensional parameter	Definition
Magnetic Reynolds number	$\mathrm{Re} = \frac{\text{Convection of B}}{\text{Diffusion of B}} = \frac{\text{Induced field}}{\text{Applied field}} = \frac{u_m D_h}{\upsilon} = \mu\sigma u_m D_h$
Reynolds number	$\mathrm{Re} = \frac{\text{Interia forces}}{\text{Viscous forces}} = \frac{u_m D_h}{\upsilon}$
Alfven number	$\mathrm{Al} = \frac{\text{Magnetic field energy}}{\text{Kinetic energy}} = \frac{\mathrm{N}}{\mathrm{Re}_m} = \frac{B^2}{\mu\rho u_m^2}$
Hartmann number	$\mathrm{Ha} = \left(\frac{\text{Electromagnetic forces}}{\text{Kinetic forces}}\right)^{1/2} = BD_h\sqrt{\sigma/\mu}$
Batchelor number (magnetic Prandtl number)	$\mathrm{Bt} \equiv \mathrm{Pr} = \frac{\mathrm{Re}_m}{\mathrm{Re}} = \mu\upsilon\sigma = \frac{\upsilon}{\upsilon_m}$
Stuart number (interaction parameter)	$\mathrm{N} \equiv \mathrm{St} = \frac{\text{Electromagnetic forces}}{\text{Interia forces}} = \frac{\mathrm{Ha}^2}{\mathrm{Re}} = \frac{\sigma B^2 D_h}{\rho u_m}$

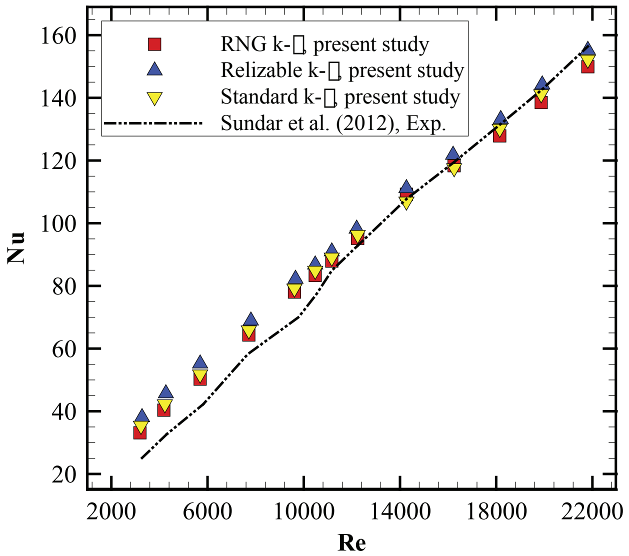

Figure 2. Code validation with experimental data of Sundar et al. [57] due to choosing the appropriate turbulent model.

[51]. Table 2 reports the most important non-dimensional parameters in MHD fluid flow.

In all simulated models during the current investigation, the HTF flow inside the HE tube is in a turbulent regime since the studied Reynolds numbers are more than 2,300. Due to simulate the resulting turbulent flow inside the absorber tube identically, separately from the continuity, momentum, and energy equations, different *k*-*ε* turbulent models equations have also been used in the ANSYS-Fluent commercial software [45].

The choice of the *k*-*ε* turbulence model is according to its wide acceptance [55]. At the same time this is successfully used in various relevant numerical studies in HEs and also our validation with experimental study of Sundar et al. [56] which is shown in Fig. 2 leaded to employing the Standard *k*-*ε* turbulent model. Fig. 2 illustrates the code validation with experimental results of Sundar et al. [56] due to choosing the appropriate turbulent model.

As it is realized in Fig. 2, the error values with Standard *k*-*ε*, Realizable *k*-*ε* and RNG *k*-*ε* models are 8.93%, 14.44%, and 9.72%, respectively. Because of the validated results of the Standard *k*-*ε* turbulent model, especially at higher Reynolds numbers, the Standard *k*-*ε* turbulent model is adopted in this work for turbulent simulation. As it is presented in the article, selected reference for comparison with the present results, is an experimental investigation. Due to selected reference, the difference between the present results and experimental data is logic. Also, the temperature dependent thermo-physical properties of HTF have been taken into account in simulations [57]. The relations which define the Standard *k*-*ε* model are as follow [58]:

$$\vec{\nabla}\left(\rho_m \vec{U}_m k\right) = \vec{\nabla}\left[\left(\mu_m + \frac{\mu_{t,m}}{\sigma_k}\right)\vec{\nabla} k\right] + G_{k,m} - \rho_m \varepsilon \quad (14)$$

$$\vec{\nabla}\left(\rho_m \vec{U}_m \varepsilon\right) = \vec{\nabla}\left[\left(\mu_m + \frac{\mu_{t,m}}{\sigma_\varepsilon}\right)\vec{\nabla}\varepsilon\right] + \frac{\varepsilon}{k}\left(c_1 G_{k,m} - c_2 \rho_m \varepsilon\right) \quad (15)$$

where $\mu_{t,m}$ is the turbulent viscosity and G is the production rate of k [60-62]:

$$\mu_{t,m} = C_\mu \rho_m \frac{k^2}{\varepsilon} \quad (16)$$

$$G_{k,m} = \mu_{t,m}\left(\vec{\nabla}\vec{U}_m + \left(\vec{\nabla}\vec{U}_m\right)^T\right) \quad (17)$$

The standard constants are employed, $C_\mu = 0.09$, $c_1 = 1.44$, $c_2 = 1.92$, $\sigma_k = 1.00$, $\sigma_\varepsilon = 1.30$ and $\sigma_t = 0.85$. The coupled steady-state governing equations have been employed, and higher-order spatial discretization arrangements have been determined. The convergence criterion value for all solver variables of the nanofluid flow and heat transfer filed is the RMS residual to be less than 10^{-6}.

As it is noted previously, the Reynolds number is defined as [44]:

$$Re = \frac{\rho_{bf} u_m D_h}{\mu_{bf}} \quad (18)$$

Where u_m refer to the fluid or nanofluid average velocity. The average Nusselt number [1] is defined as:

$$Nu_{av} = \frac{h_{bf} D_h}{k_{bf}} \quad (19)$$

The pressure drop between the inlet and outlet of the test section [44]:

$$\Delta p = p_{av,inlet} - p_{av,outlet} \quad (20)$$

The friction factor coefficient for fully developed flow is computed as [1]:

$$f = \frac{2}{\left(\frac{L_2}{D_h}\right)} \frac{\Delta p}{\rho_{hnf} {u_m}^2} \quad (21)$$

The thermal and hydraulic performance evaluation criterion (PEC) is defined in order to compare the overall hydrothermal performance of corrugated and plain HE, which is obtained as follows [1]:

$$PEC = \left(\frac{Nu_{av}}{Nu_{av,s}}\right)\left(\frac{f}{f_s}\right)^{-1/3} \quad (22)$$

where Nu_{av} and $Nu_{av,s}$ are the predicted mean Nusselt number for the corrugated and plain HE. Additionally, f and f_s are the predicted mean friction factors for the corrugated and plain HE.

Table 3. The thermophysical properties of the Newtonian base fluid and solid nanoparticles at T = 300 K [63, 64].

Material	ρ (kg/m³)	c_p (J/kg·K)	k (W/m·K)	μ (N·s/m²)
H_2O	997.1	4179	0.6	0.00339
Fe_2O_3	5200	670	6	-

Nanofluid

The considered Newtonian ferro-nanofluid in the current investigation is Fe_2O_3/H_2O. To achieve the most efficient Newtonian nanofluid in the present study, the solid nanoparticles of Fe_2O_3 at volume concentration of $\phi = 1$ % are added to the base fluid with a mean predicted diameter of 20 nm. Table 3 reports the thermophysical properties of the Newtonian base fluid and solid particles.

The nanofluid effective density ρ_{nf} and specific heat capacity $C_{p,nf}$ of the thermal Fe_2O_3/H_2O ferro-nanofluid, are determined using the following equations, where ϕ is the volume concentration [62, 63].

$$\rho_{nf} = \phi\rho_{np} + (1-\phi)\rho_{bf} \tag{23}$$

$$(\rho c_p)_{nf} = \phi(\rho c_p)_{np} + (1-\phi)(\rho c_p)_{bf} \tag{24}$$

Also, the effective thermal conductivity and dynamic viscosity of the Fe_2O_3/H_2O ferro-nanofluid can be calculated using the following equations [63-66].

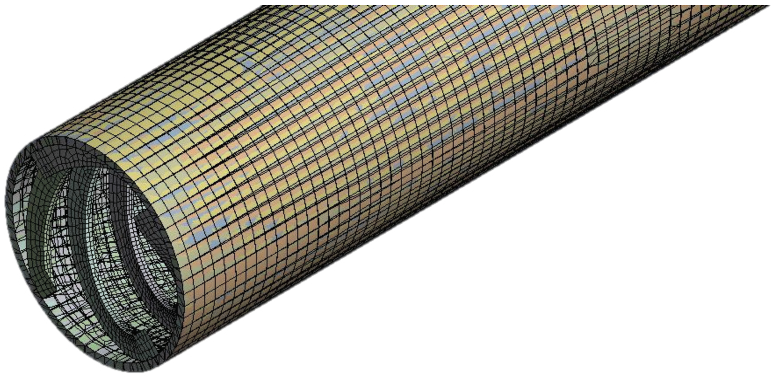

(a)

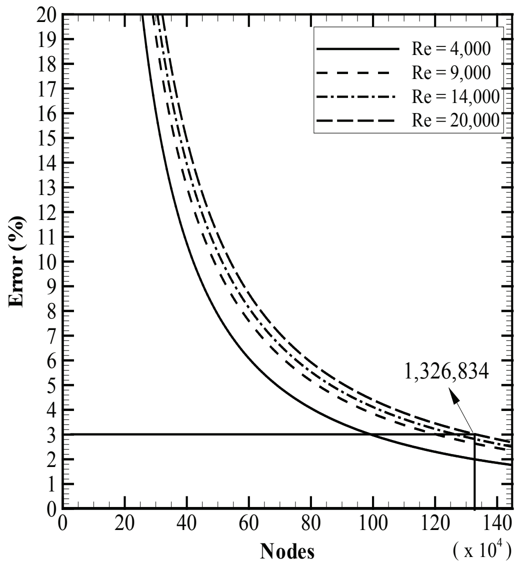

(b)

Figure 3. (a) Grid mesh layout of the pipe wall and (b) grid independence test in the present study for different Reynolds numbers for a model with $b = 6$ mm, $r = 5$ mm and $p = 12.5$ mm filled with nanofluid at $\phi = 1\%$.

$$k_{nf} = \frac{k_{np} + 2k_{bf} - 2\phi(k_{bf} - k_{np})}{k_{np} + 2k_{bf} + \phi(k_{bf} - k_{np})} k_{bf} \quad (25)$$

$$\mu_{nf} = (3.1000B + 0.0350B^2 + 4263.0200\phi - 27886.4807\phi^2 + 316.0629)e^{-0.0200T} \quad (26)$$

To simulate the Fe_2O_3/H_2O ferro-nanofluid flow through a HE, the *Eulerian-Eulerian Two-Phase Mixture Model* (TPM) is employed in the current investigation [45]. The TPM supposes that the phases-coupling is strong, and particles nearly track the interruption flow [46]. The two-phases (solid nanoparticles and base fluid) are assumed to be interpenetrating, which funds that every phase has a certain value of velocity field. Also, there is a volume concentration of fluid phase in every control volume and another volume fraction (ϕ) for the nanoparticle phase. This model is illustrated to give powerful estimating, even for low nanoparticle volume fractions [47].

Validation

Grid independency test

Fig. 3 illustrates the grid mesh layout of the pipe wall and the grid independence test in the present study for different Reynolds numbers for a model with b = 6 mm, r = 5 mm, and p = 12.5 mm filled with nanofluid at ϕ = 1%.

As shown in Fig. 3b, a grid independence test was performed for the corrugated pipe using nanofluid to analyze the effects of grid sizes on the results. By comparing the results, it is concluded that mesh configurations contains a grid number of 1,326,834 nodes is assumed to get a satisfactory agreement between the computational time and the accuracy of results with the maximum error of 3%.

Code validation

Also, the computational fluid dynamics (CFD) code validation was done by comparing of numerical results obtained from the present study and experimental data of Sha et al. [63]. Fig. 4 shows this code validation with experimental data of Sha et al. [64] versus Reynolds numbers and magnetic fields. It can be realized from this figure that a remarkable agreement exists among the empirical data of Sha et al. [63] and numerical results obtained from the present study employing TPM. It is seen that the TPM simulation in the present work leads to an appropriate validation with the experimental data during all studied Reynolds numbers and magnetic fields.

RESULTS AND DISCUSSION

Usage of Corrugations and Nanofluid

In this section, the thermal-hydraulic analysis of Basic HE (B.HE) filled with Base Fluid (BF), Corrugated HE (C.HE) filled with BF, B.HE filled with Nanofluid (NF) and C.HE filled with NF has been done.

Fig. 5 illustrates the average predicted Nusselt number versus Reynolds numbers for B.HE and C.HE (b = 6 mm, r = 5 mm and p = 12.5 mm) which are filled with BF or NF (ϕ = 1%) under no magnetic field (B = 0).

As it is seen in this figure, usage of C.HE (filled with BF or NF) can increase the average Nusselt number in tube the significantly. The presence of ribs can destroy the laminar sub-layers in HE and generate local vortexes, enhancing the flow mixing in fluid flow. This phenomenon leads to a higher heat transfer coefficient in HE and therefore increases the Nusselt number values. Also, it is found that usage of NF (for both B.HE and C.HE) can increase the

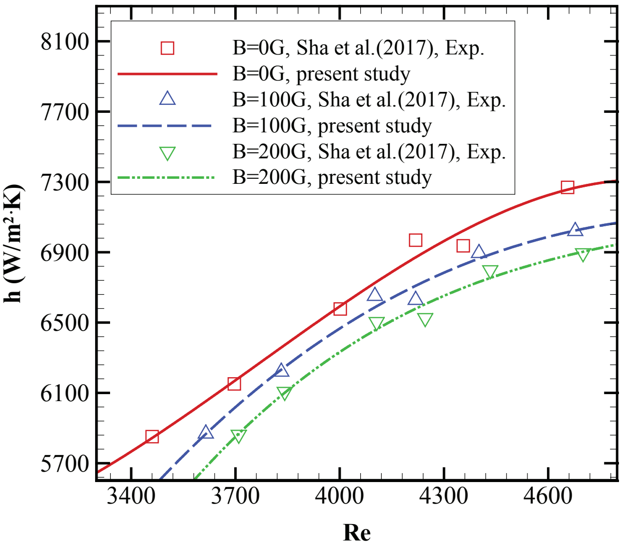

(a)

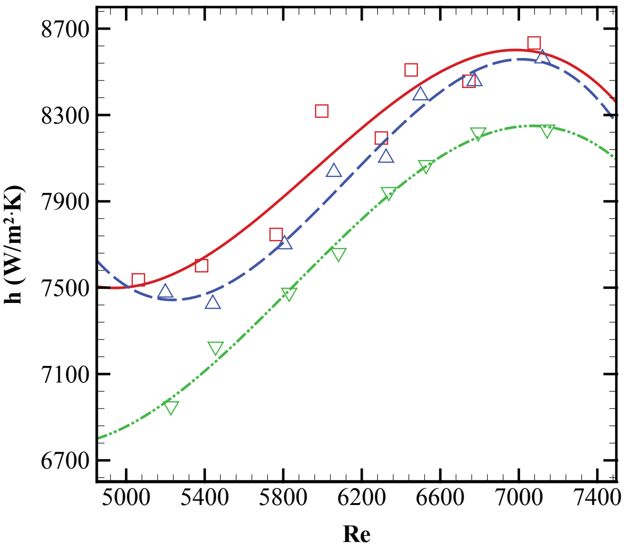

(b)

Figure 4. Code validation with the experimental data of Sha et al. [63] versus Reynolds numbers and magnetic fields.

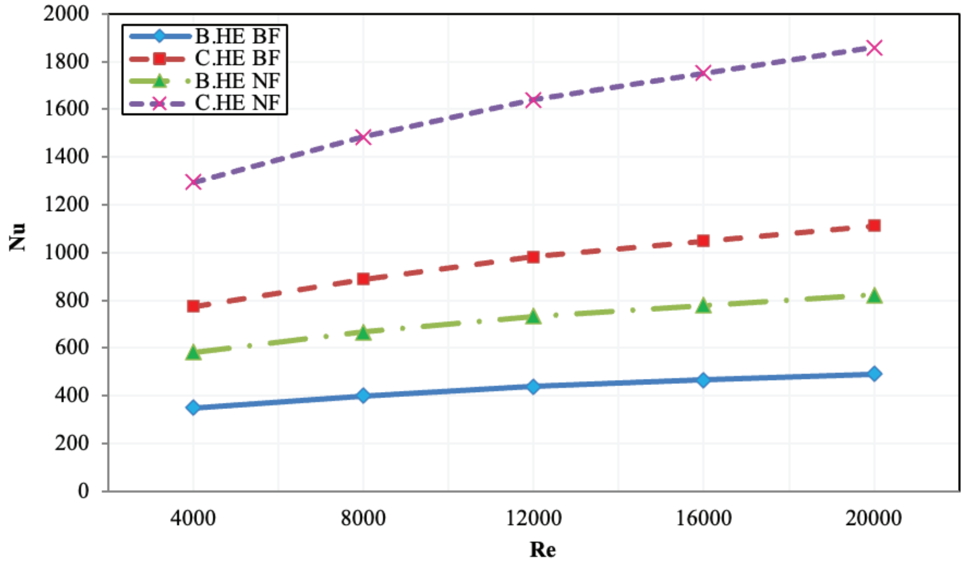

Figure 5. Average predicted Nusselt number versus Reynolds number for B.HE and C.HE (b = 6 mm, r = 5 mm and p = 12.5 mm) which are filled with BF or NF (ϕ = 1%) under no magnetic field (B = 0).

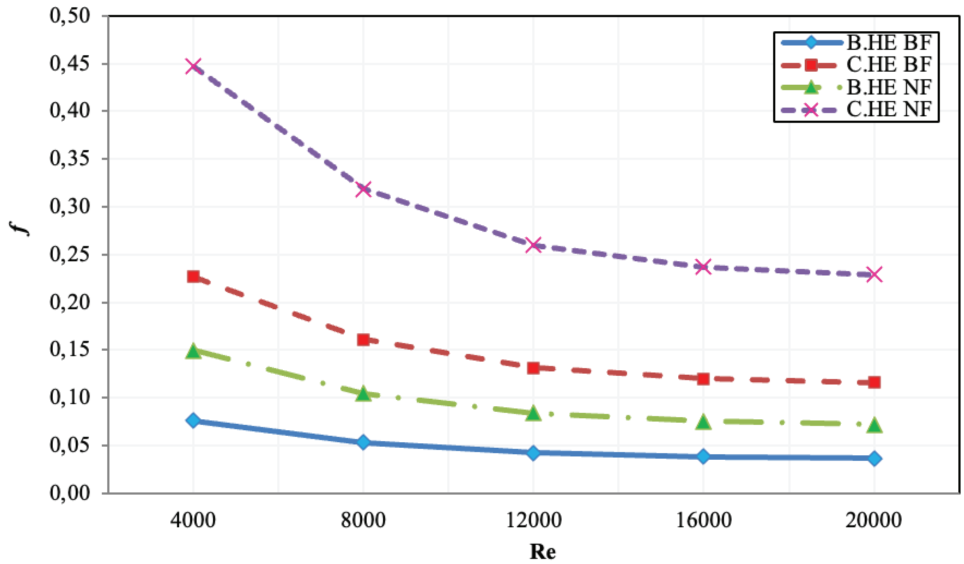

Figure 6. Mean predicted friction factor versus Reynolds number for B.HE and C.HE (b = 6 mm, r = 5 mm and p = 12.5 mm) which are filled with BF or NF (ϕ = 1%) under no magnetic field (B = 0).

average Nusselt number in the tube sharply. Nanofluids have higher thermal conductivity value than base fluids, and it leads to a higher heat transfer coefficient in HE and therefore increases the Nusselt number values. Besides, it is realized that for all studied configurations and models, the average Nusselt number always increases by an increase of Reynolds numbers. Higher Reynolds number related to higher flow velocities, leading to more flow mixing, vortex generation, and local turbulence in HE and hence increase the heat transfer coefficient in the tube. It is observed that the C.HE filled with NF has the highest Nusselt number values among all studied cases. During all investigated Reynolds numbers, which is followed with cases C.HE filled with BF, B.HE filled with NF and B.HE filled with BF, respectively. The usage of C.HE filled with BF is more efficient than using B.HE filled with NF.

Fig. 6 presents the mean predicted friction factor versus Reynolds number for B.HE and C.HE (b = 6 mm, r = 5 mm and p = 12.5 mm) which are filled with BF or NF (ϕ = 1%) under no magnetic field (B = 0). As is seen in this figure,

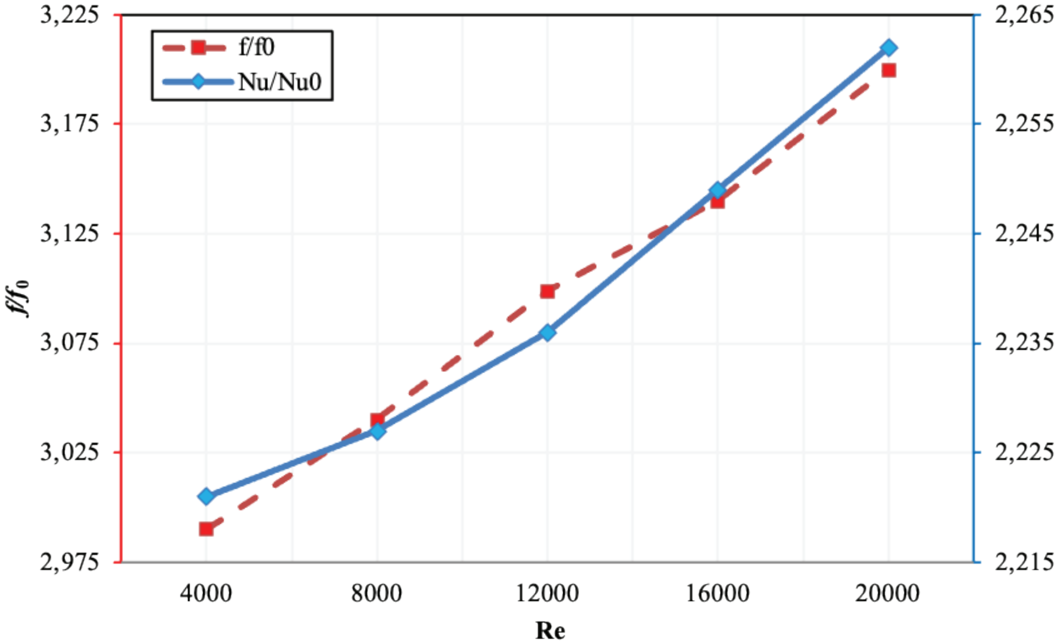

Figure 7. Nusselt number ratio and friction factor ratio versus Reynolds number for C.HE (b = 6 mm, r = 5 mm and p = 12.5 mm) which is filled with NF (ϕ = 1%) and under no magnetic field (B = 0) in comparison with B.HE filled with NF (ϕ = 1%) under no magnetic field (B = 0).

usage of C.HE (filled with BF or NF) can increase the mean friction factor in the tube significantly.

The presence of ribs can destroy the laminar sub-layers in HE and generate local vortexes, increasing the flow mixing in fluid flow. This phenomenon leads to a higher pressure drop penalty from inlet to outlet of test section in HE and therefore increases the friction factor values.

Also, it is found that usage of NF (for both B.HE and C.HE) can increase the mean friction factor in the tube sharply. Nanofluids have higher dynamic viscosity values than base fluids, and it leads to a higher pressure drop penalty in HE and therefore increases the friction factor values. Besides, it is realized that for all studied configurations and models, the mean friction factor always decreases by an increase of Reynolds numbers. It is observed that the C.HE filled with NF has the highest friction factor values among all studied cases. During all investigated Reynolds numbers, which is followed with C.HE filled with BF, B.HE filled with NF and B.HE filled with BF, respectively. It is interesting that utilizing C.HE filled with BF leads to more friction factor values than using B.HE filled with NF.

Fig. 7 demonstrates Nusselt number ratio and friction factor ratio versus Reynolds number for C.HE (b = 6 mm, r = 5 mm and p = 12.5 mm) which is filled with NF (ϕ = 1%) and under no magnetic field (B = 0) in comparison with B.HE filled with NF (ϕ = 1%) under no magnetic field (B = 0). As is seen in this figure, both Nusselt number and friction factor ratios always increase by the increase of Reynolds numbers. In the next section, the PEC values are calculated to analyze the thermal-hydraulic characteristics of HE.

Applying of Magnetic Field

Fig. 8 shows the average predicted Nusselt number versus Reynolds number for B.HE and C.HE (b = 6 mm, r = 5 mm and p = 12.5 mm) which is filled with NF (ϕ = 1%) under various magnetic fields (B = 0, 200 G, 400 G and 600 G). As is seen in Fig. 8a, usage of C.HE in the absence of magnetic field can increase the average Nusselt number in the tube significantly. Besides, it is realized that for all studied configurations and models, the average Nusselt number always increases by an increase of Reynolds numbers.

It is observed that the C.HE filled with NF can enhance the Nusselt number value than B.HE filled with NF about 122.1% at Re = 4,000 and about 126.2% at Re = 20,000. Fig. 8b illustrates that usage of C.HE in presence of a magnetic field (B = 200 G) can increase the average Nusselt number in the tube sharply. Moreover, it is found that for all studied configurations and models, the average Nusselt number always increases by an increase of Reynolds numbers. It is clearly observed that the C.HE filled with NF can enhance the Nusselt number value than B.HE filled with NF about 122.3% at Re = 4,000 and about 126.5% at Re = 20,000. As it is observed in Fig. 8c, usage of C.HE in presence of a magnetic field (B = 400 G) can increase the average Nusselt number in the tube sharply. Moreover, it is found that for all studied configurations and models, the average Nusselt number always increases by an increase of Reynolds numbers. It is observed that the C.HE filled with

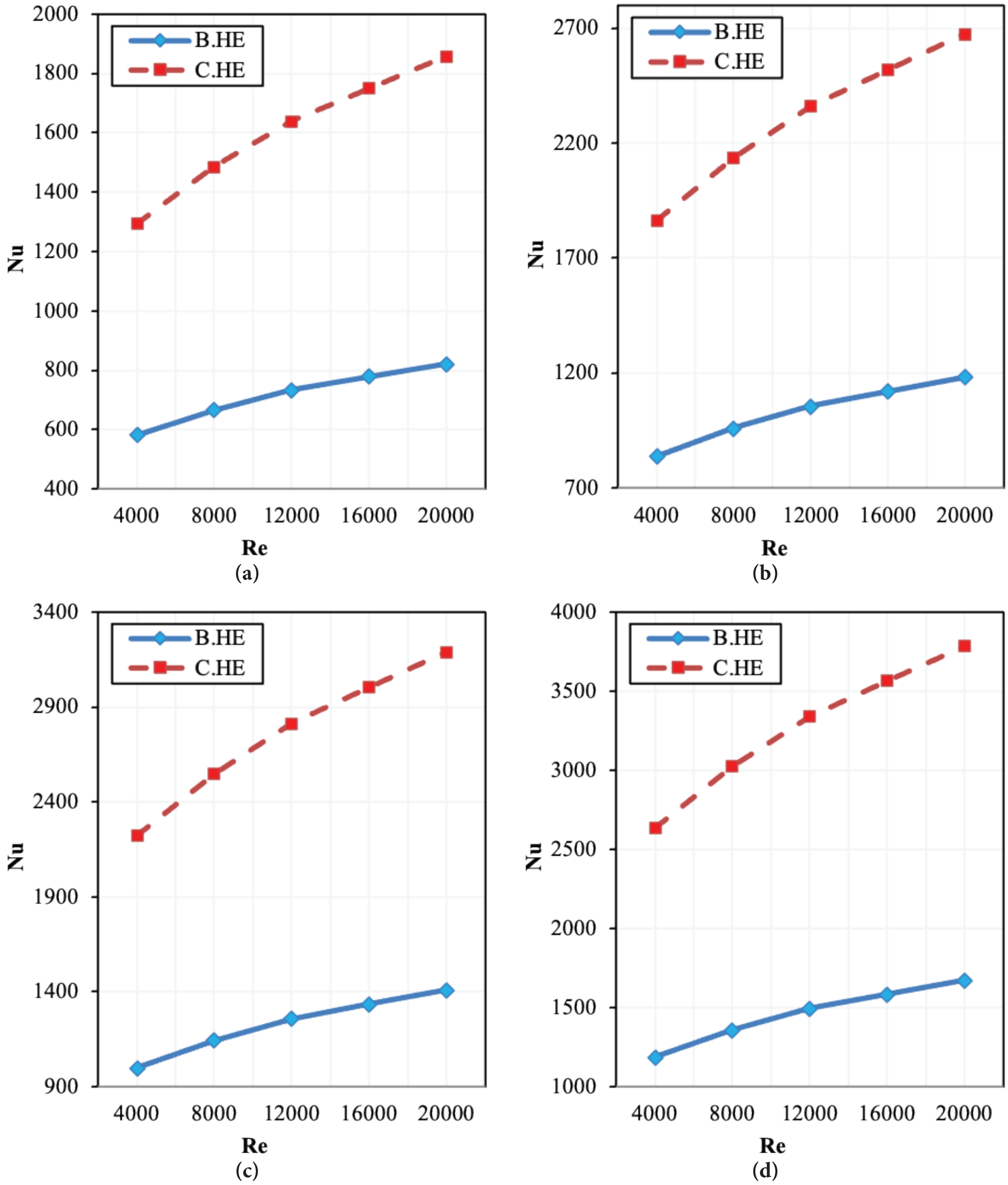

Figure 8. Average Nusselt number versus Reynolds number for B.HE and C.HE (b = 6 mm, r = 5 mm and, p = 12.5 mm) which is filled with NF (ϕ = 1%) under various magnetic fields (B = 0, 200 G, 400 G and 600 G).

NF can enhance the Nusselt number value than B.HE filled with NF about 122.5% at Re = 4,000 and about 126.7% at Re = 20,000. Fig. 8d demonstrates that the usage of C.HE in presence of a magnetic field (B = 600 G) can increase the average Nusselt number in the tube sharply. Moreover, it is found that for all studied configurations and models, the average Nusselt number always increases by an increase of Reynolds numbers. It is observed that the C.HE filled with NF can enhance the Nusselt number value than B.HE filled with NF about 122.7% at Re = 4,000 and about 126.8% at Re = 20,000.

Fig. 9 shows Nusselt number ratio versus Reynolds number for C.HE (b = 6 mm, r = 5 mm, p = 12.5 mm) which is filled with NF (ϕ = 1%) and under various magnetic fields (B = 0, 200 G, 400 G and 600 G) in comparison with B.HE filled with NF (ϕ = 1%) and under no magnetic field (B = 0). It is understood that the presence of a magnetic field has a significant effect on heat transfer enhancement in HE. Also, it is found that higher magnetic field intensities can enhance the heat transfer rate in HE. The model with a magnetic field of B = 600 G has the highest Nusselt number ratio among all studied models, which is followed with models B = 400 G, 200 G, and 0, respectively. It is observed that the C.HE filled with NF at B = 600 G can enhance the Nusselt number ratio than C.HE filled with NF at B = 0 about 103.6% at Re = 4,000 and about 103.5% at Re = 20,000.

Geometrical Parameters of Corrugations

In this section, the reference data due to calculating Nu_0, f_0, and PEC index are achieved from B.HE filled with NF at ϕ = 1%.

Different corrugation heights

Fig. 10 shows effects of different corrugation heights on (a) Nusselt number ratio, (b) friction factor ratio and (c) PEC versus Reynolds number for C.HE (r = 5 mm and p = 12.5 mm) which is filled with NF (ϕ = 1%) and under magnetic field B = 600 G in comparison with B.HE filled with NF (ϕ = 1%) under no magnetic field (B = 0). As is seen in Fig. 10a, corrugation heights can affect the thermal characteristics of HE significantly. The configuration with b = 14 mm has the highest Nusselt number ratios among all studied cases during all studied Reynolds number and is followed with configurations heigh of b = 10 and 6 mm, respectively. It is clear that the increase of corrugation heights leads to more flow mixing and vortexes generation in HE and therefore enhances the heat transfer coefficient between tube wall and HTF. Besides, it is realized that for all studied configurations and models, the average Nusselt number ratio always increases by an increase of Reynolds numbers. Fig. 10b demonstrates that corrugation heights can affect the hydraulic characteristics of HE significantly. The configuration with b = 14 mm has the highest friction factor ratios among all studied cases during all studied Reynolds number and is followed with configurations b = 10 and 6 mm, respectively. It is clear that the increase of corrugation heights leads to more flow mixing and vortexes generation in HE and therefore increases the pressure drop penalty from inlet to outlet of the test section.

Besides, it is realized that for all studied configurations and models, the mean friction factor ratio always increases by an increase of Reynolds numbers. Fig. 10c illustrates that corrugation heights can affect the thermal-hydraulic characteristics of HE significantly. The configuration with b = 14 mm has the highest PEC values among all studied cases during all studied Reynolds number and is followed with configurations height of b = 10 and 6 mm, respectively. It is clear that the increase of corrugation heights leads to more flow mixing and vortexes generation in HE and therefore increases the both parameters as heat transfer coefficient and pressure drop penalty from inlet to outlet of the test section. The PEC index calculates which parameter plays

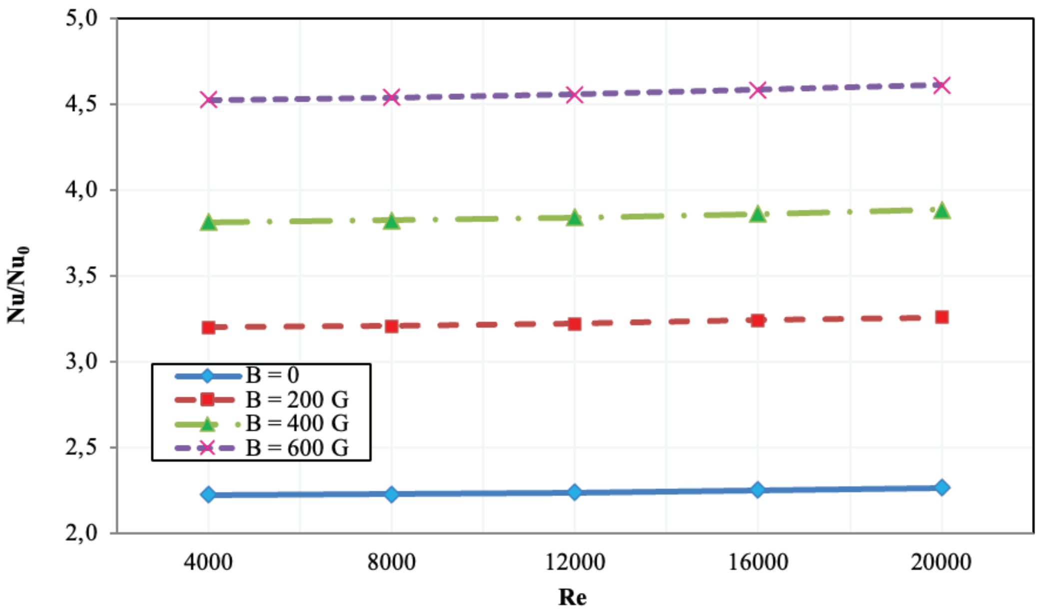

Figure 9. Nusselt number ratio versus Reynolds number for C.HE (b = 6 mm, r = 5 mm and p = 12.5 mm) which is filled with NF (ϕ = 1%) and under various magnetic fields (B = 0, 200 G, 400 G and 600 G) in comparison with B.HE filled with NF (ϕ = 1%) under no magnetic field (B = 0).

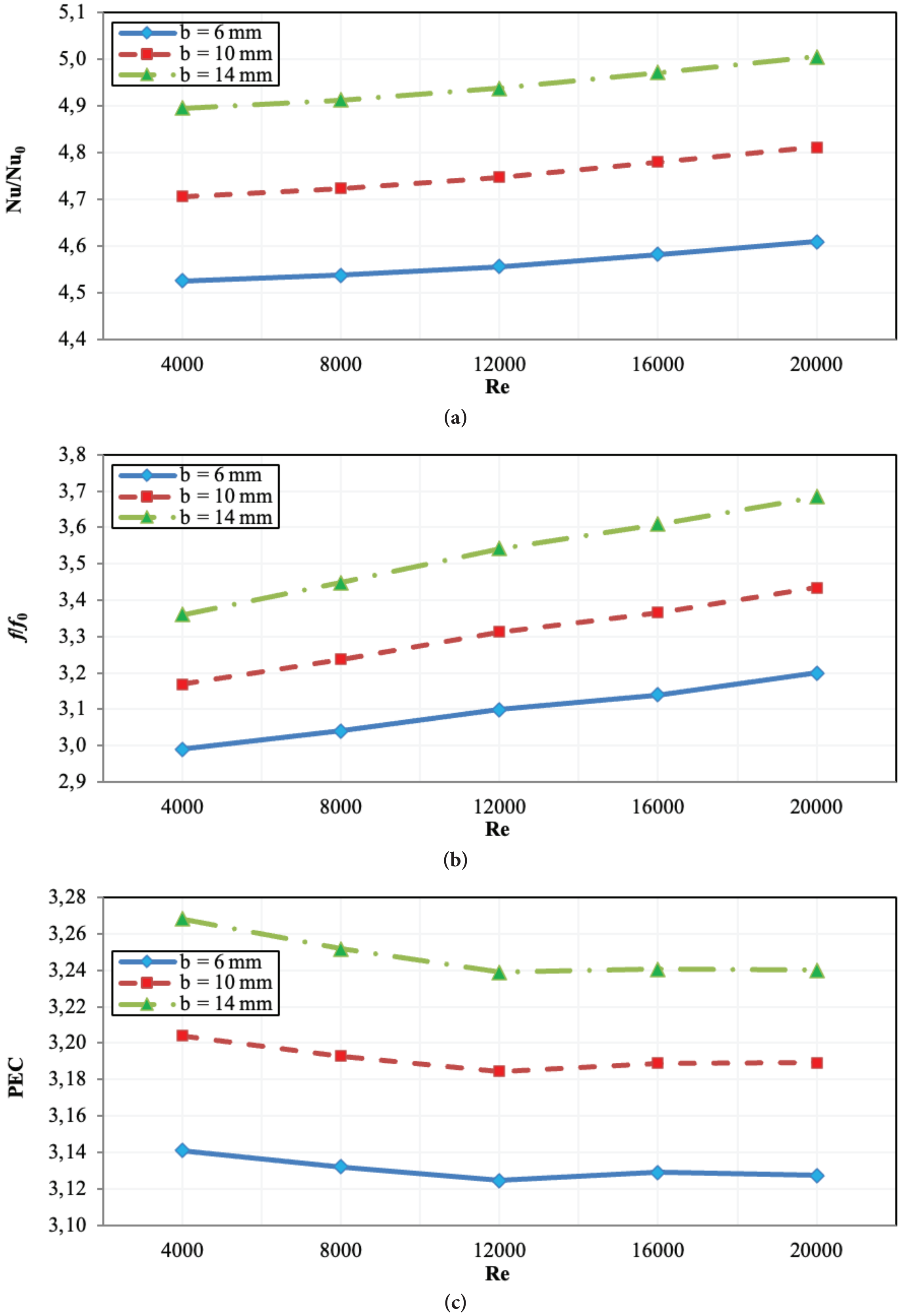

Figure 10. Effects of corrugation heights on (a) Nusselt number ratio, (b) friction factor ratio and (c) PEC versus Reynolds number for C.HE (r = 5 mm and p = 12.5 mm) which is filled with NF (ϕ = 1%) under magnetic field B = 600 G in comparison with B.HE filled with NF (ϕ = 1%) under no magnetic field (B = 0).

the main role in HE, Nusselt number enhancement, or pressure drop penalty. Besides, it is realized that for all studied configurations and models, the PEC variations have similar trends with each other versus Reynolds numbers. The PEC values reduce by increase of Reynolds number from Re = 4,000 to Re = 12,000, and then increase till Re = 16,000 and then once again decrease till Re = 20,000. In some regions of Reynolds number the Nusselt number plays the main role (12,000 < Re < 16,000) and in some other regions of Reynolds number the friction factor plays the main role (4,000 < Re < 12,000 and 16,000 < Re < 20,000). Also the highest PEC values are achieved in Re = 4,000. The most PEC value in this figure is PEC = 3.2680 for C.HE (b = 14 mm, r = 5 mm and p = 12.5 mm) which is filled with NF (ϕ = 1%) and under magnetic field B = 600 G at Re = 4,000. In the rest of present study the corrugation height of b = 14 mm is determined for analyzing of other parameters.

Different corrugation widths

Fig. 11 presents effects of different corrugation widths on (a) Nusselt number ratio, (b) friction factor ratio and (c) PEC versus Reynolds number for C.HE (b = 14 mm and p = 12.5 mm) which is filled with NF (ϕ= 1%) under magnetic field B = 600 G in comparison with B.HE filled with NF (ϕ = 1%) under no magnetic field (B = 0). As it is realized in Fig. 11a, corrugation widths can affect the thermal characteristics of HE sharply. The configuration with r = 13 mm has the highest Nusselt number ratios among all studied cases during all studied Reynolds number and is followed with configurations r = 9 and 5 mm, respectively. It is clear that the increase of corrugation widths leads to more flow mixing and vortexes generation in HE and therefore enhances the heat transfer coefficient between the tube wall and HTF. Besides, it is realized that for all studied configurations and models, the average Nusselt number ratio always increases by an increase of Reynolds numbers. Fig. 11b demonstrates that corrugation widths can affect the hydraulic characteristics of HE significantly. The configuration with r = 13 mm has the highest friction factor ratios among all studied cases during all studied Reynolds number and is followed with configurations width of r = 9 and 5 mm, respectively. It is clear that the increase of corrugation widths leads to more flow mixing and vortexes generation in HE and therefore increases the pressure drop penalty from inlet to outlet of the test section. Besides, it is realized that for all studied configurations and models, the mean friction factor ratio always increases by an increase of Reynolds numbers. Fig. 11c illustrates that corrugation widths can affect the thermal-hydraulic characteristics of HE. The configuration with width r = 9 mm has the highest PEC values among all studied cases during all studied Reynolds number and is followed with configurations width r = 13 and 5 mm, respectively.

It is clear that the increase of corrugation widths leads to more flow mixing and vortexes generation in HE and therefore increases both parameters heat transfer coefficient and pressure drop penalty from inlet to outlet of the test section. The PEC index calculates which parameter plays the main role in HE, Nusselt number enhancement, or pressure drop penalty. Here the configuration width r = 13 mm has the highest Nusselt number values, but because of its high-pressure drop values cannot achieve the highest PEC values. Therefore, the configuration width r = 9 mm is in the first place. Besides, it is realized that for all studied configurations and models, the PEC variations have similar trends with each other versus Reynolds numbers. The PEC values reduce by increase of Reynolds number from Re = 4,000 to Re = 12,000, and then increase till Re = 16,000 and then once again decrease till Re = 20,000. For configuration width of r = 9 mm the PEC values increase in Reynolds number period from 16,000 to 20,000. In some regions of Reynolds number the Nusselt number plays the main role (12,000 < Re < 16,000) and in some other regions of Reynolds number the friction factor plays the main role (4,000 < Re < 12,000 and 16,000 < Re < 20,000). Also, the highest PEC values are achieved in Re = 4,000. The most PEC value in this figure is PEC = 3.3024 for C.HE (b = 14 mm, r = 9 mm and p = 12.5 mm) which is filled with NF (ϕ = 1%) under magnetic field B = 600 G at Re = 4,000. In the rest of the study the corrugation height of b = 14 mm and corrugation width of r = 9 mm is determined for analyzing of the pitch value parameter.

Different corrugation pitches

Fig. 12 demonstrates effects of different corrugation pitches on (a) Nusselt number ratio, (b) friction factor ratio and (c) PEC versus Reynolds number for C.HE (b = 14 mm and r = 9 mm) which is filled with NF (ϕ = 1%) under magnetic field B = 600 G in comparison with B.HE filled with NF (ϕ = 1%) under no magnetic field (B = 0). As it is realized in Fig. 12a, corrugation pitches can affect the thermal characteristics of HE significantly. The configuration with pitch p = 12.5 mm has the highest Nusselt number ratios among all studied cases during all studied Reynolds number and is followed with configurations pitch p = 20.0 and 27.5 mm, respectively. It is clear that the decrease of corrugation pitches leads to more flow mixing and vortexes generation in HE and therefore enhances the heat transfer coefficient between the tube wall and HTF. Besides, it is realized that for all studied configurations and models, the average Nusselt number ratio always increases by an increase of Reynolds numbers. Fig. 12b demonstrates that corrugation pitches can also affect the hydraulic characteristics of HE. The configuration pitch with p=12.5 mm has the highest friction factor ratios among all studied cases during all studied Reynolds number and is followed with configurations pitch p = 20.0 and 27.5 mm, respectively. It is clear that reduction of corrugation pitches leads to more flow mixing and vortexes generation in HE and therefore increases the pressure drop penalty from inlet to outlet of the test section. Besides, it is realized that for all studied configurations and models, the mean friction factor ratio

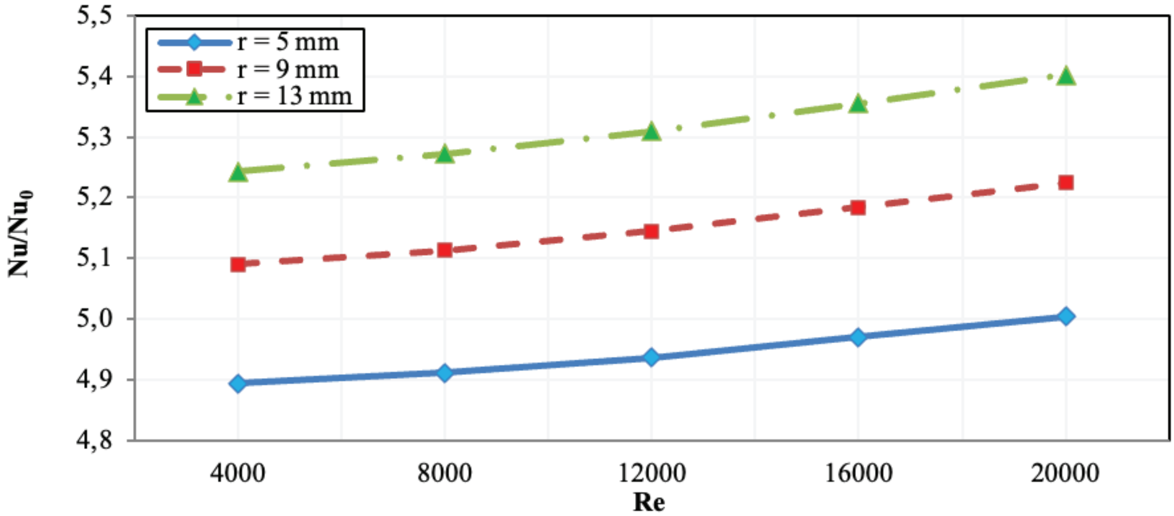

(a)

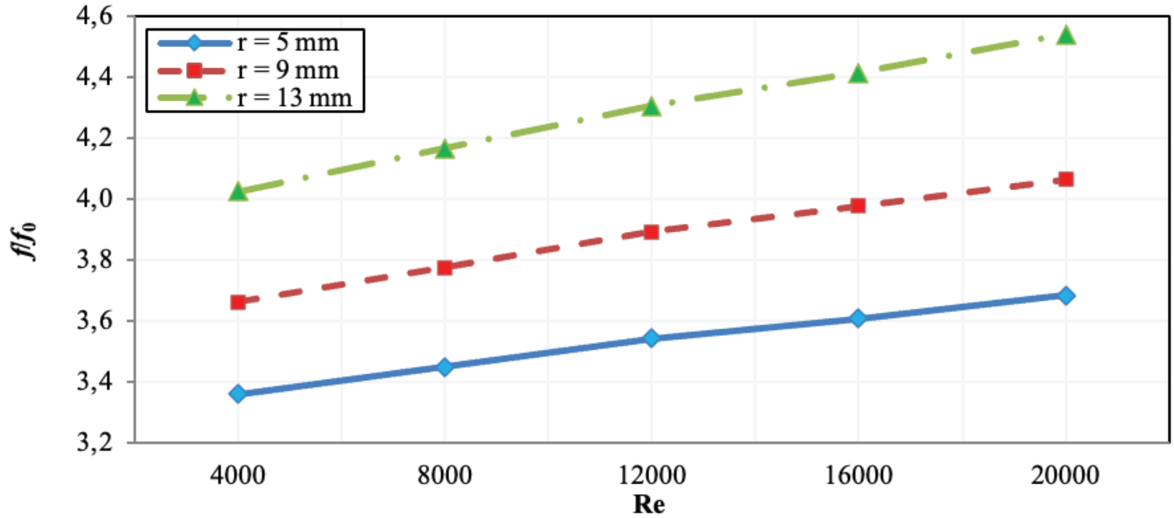

(b)

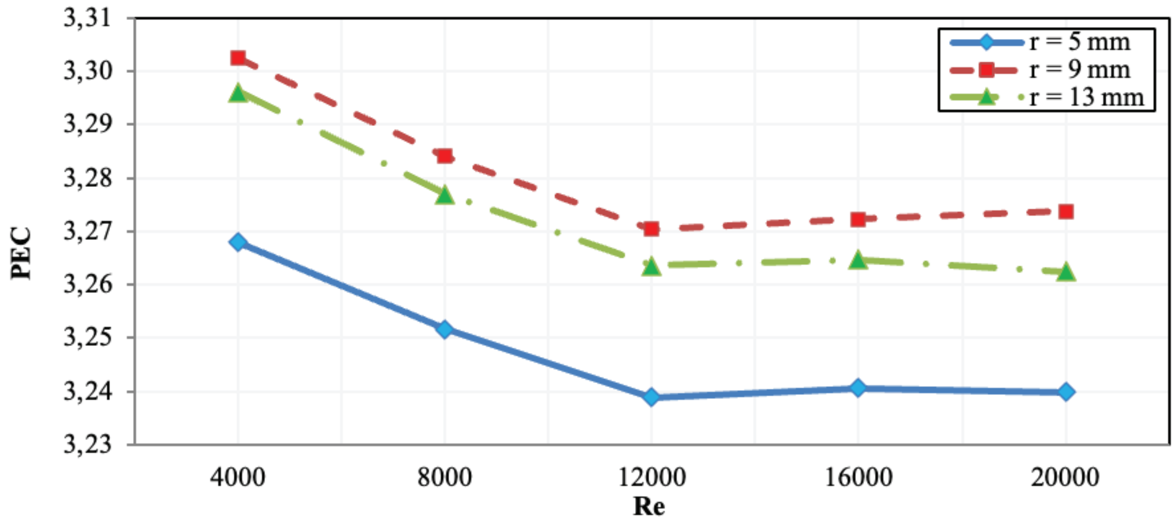

(c)

Figure 11. (a) Nusselt number ratio, (b) friction factor ratio and (c) PEC versus Reynolds number for C.HE (b = 14 mm and p = 12.5 mm) which is filled with NF (ϕ = 1%) under magnetic field B = 600 G in comparison with B.HE filled with NF (ϕ = 1%) under no magnetic field (B = 0) for various corrugation widths.

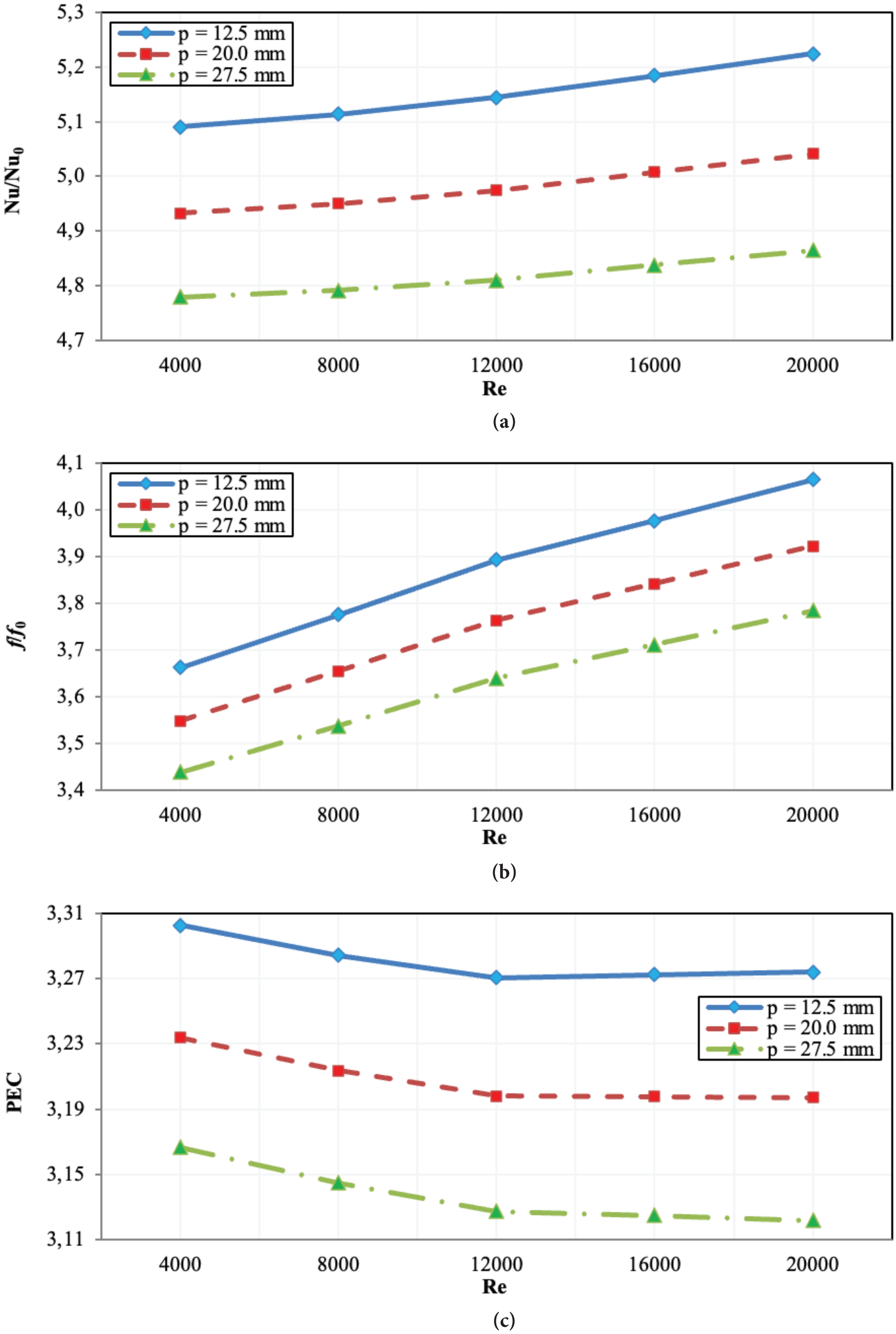

Figure 12. (a) Nusselt number ratio, (b) friction factor ratio and (c) PEC versus Reynolds number for C.HE (b = 14 mm and r = 9 mm) which is filled with NF (ϕ = 1%) under magnetic field B= 600 G in comparison with B.HE filled with NF (ϕ = 1%) under no magnetic field (B = 0) for various corrugation pitch.

always increases by an increase of Reynolds numbers. Fig. 12c illustrates that corrugation pitches can affect the thermal-hydraulic characteristics of HE. The configuration pitch with p=12.5 mm has the highest PEC values among all studied cases during all studied Reynolds number and is followed with configurations pitch of p=20.0 and 27.5 mm, respectively. It is clear that the decrease of corrugation pitches leads to more flow mixing and vortexes generation in HE and therefore increase both parameters heat transfer coefficient and pressure drop penalty from inlet to outlet of the test section. The PEC index calculates which parameter plays the main role in HE, Nusselt number enhancement, or pressure drop penalty. Here the configuration pitch p = 12.5 mm has the highest Nusselt number values and also the highest pressure drop values and also has the highest PEC values.

Besides, it is realized that for all studied configurations and models, the PEC variations have similar trends with each other versus Reynolds numbers. The PEC values reduce by an increase of Reynolds number from Re = 4,000 to Re = 12,000 with an almost high slop and then decrease till Re = 20,000 slower. For configuration pitch p = 12.5 mm the PEC values increase in Reynolds number period from 12,000 to 20,000. In this region of Reynolds number the Nusselt number plays the main role (12,000 < Re < 16,000), while in other regions of Reynolds number the friction factor plays the main role (4,000 < Re < 12,000). Also, the highest PEC values are achieved in Re = 4,000. The most PEC value in this figure is PEC = 3.3024 for C.HE (b = 14 mm, r = 9 mm and p = 12.5 mm) which is filled with NF (ϕ = 1%) under magnetic field B = 600 G at Re = 4,000.

Finally, usage of C.HE (b = 14 mm, r = 9 mm and p = 12.5 mm), which is filled with NF (ϕ = 1%) and under magnetic field B = 600 G it suggested in the present study as the most thermal-hydraulic-efficient configuration. Also, there is a Reynolds number (Re = 4,000), in which the highest PEC values are achieved.

It is valuable to refer that, the PEC is evaluated with estimated Nusselt number and friction factor. As it is clear, the trends of Nusselt number and friction factor determine the trend of PEC. As one can see in Fig. 10, 11 and 12, the trends of Nusselt number and friction factor in each figure are similar for various value of used parameters.

CONCLUSION

This paper studied the effects of using a magnetic field on the flow field and heat transfer of ferromagnetic Fe_3O_4/H_2O nanofluid with consideration of a two-phase model for nanofluid in heat exchanger equipped with helical ribs. The length of the heat exchanger is 200.0 mm, and the tube diameter is 50.0 mm. Also, the inlet length of 830.0 mm and outlet length of 66.0 mm are determined. Besides, four different constant magnetic fields (B = 0, 200, 400, and 600 G) are determined to analyze the effects of employing MHD fluid flow in heat exchanger under the magnetic field. The heat transfer fluid is Fe_3O_4/H_2O nanofluid at a nanoparticles volume fraction of ϕ = 1.0% and diameter of d_{np} = 20 nm. Also effects of changing three geometrical parameters are analyzed: Three different corrugation height values (b = 6.0, 10.0 and 14.0), three different corrugation width values (r = 5.0, 9.0 and 13.0) and three different corrugation pitch values (p = 12.5, 20.0 and 27.5). The performance evaluation criteria index is employed to analyze the thermal-hydraulic characteristics of the heat exchanger. Based on the obtained results,

- Usage of the corrugated heat exchanger or nanofluid can increase the average Nusselt number and friction factor in the tube sharply.
- It is understood that the presence of a magnetic field has a significant effect on heat transfer enhancement in the heat exchanger.
- The model with magnetic field 600 G has the highest Nusselt number ratio among all studied models, which is followed with 400 G, 200 G, and 0 magnetic fields, respectively.
- Effects of different corrugation heights, widths, and pitches have been studied.
- Usage of the novel corrugated heat exchanger with 14 mm corrugation heights, 9 mm rib width, and 12.5 mm blade pitches filled with nanofluid and under a magnetic field of 600 G it suggested in the present study as the most thermal-hydraulic-efficient configuration.
- At the Reynolds number of 4,000, the highest performance evaluation criteria values are achieved.

DECLARATIONS

The authors declare that they have no known competing financial interests or personal relationships that could have appeared to influence the work reported in this paper.

AUTHORSHIP CONTRIBUTIONS

Authors equally contributed to this work.

DATA AVAILABILITY STATEMENT

The authors confirm that the data that supports the findings of this study are available within the article. Raw data that support the finding of this study are available from the corresponding author, upon reasonable request.

CONFLICT OF INTEREST

The author declared no potential conflicts of interest with respect to the research, authorship, and/or publication of this article.

ETHICS

There are no ethical issues with the publication of this manuscript.

REFERENCES

[1] Abbasian Arani AA, Sadripour S, Kermani S. Nanoparticle shape effects on thermal-hydraulic performance of boehmite alumina nanofluids in a sinusoidal-wavy mini-channel with phase shift and variable wavelength. Int J Mech Sci 2017;128–129:550-563. [CrossRef]

[2] Ali MM, Alim A, Ahmed SS. Finite element solution of hydromagnetic mixed convection in a nanofluid filled vented grooved channel. J Ther Eng 2021;7:91−108. [CrossRef]

[3] Güllüce H, Özdemir K. Design and operational condition optimization of a rotary regenerative heat exchanger. Appl Therm Eng 2020;177:115341. [CrossRef]

[4] Ahmadpour V, Rezazadeh S, Mirzaei I, Mosaffa AH. Numerical investigation of horizontal magnetic field effect on the flow characteristics of gallium filled in a vertical annulus. J Ther Eng 2021;7:984–999. [CrossRef]

[5] Sadripour S. 3D numerical analysis of atmospheric-aerosol/carbon-black nanofluid flow within a solar air heater located in Shiraz, Iran. Int J Numer Method Heat Fluid Flow 2019;29:1378−1402. [CrossRef]

[6] Sobamowo MG, Adesina AO. Thermal performance analysis of convective-radiative fin with temperature-dependent thermal conductivity in the presence of uniform magnetic field using partial noether method. J Ther Eng 2018;4:2287–2302. [CrossRef]

[7] Ali Aljubury IM, Hussain MK, Farhan A. The optimal geometric design of a v-corrugated absorber solar air heater integrated with twisted tape inserts. J Ther Eng 2023;9:478–496. [CrossRef]

[8] Bayareh M, Nourbakhsh A. Numerical simulation and analysis of heat transfer for different geometries of corrugated tubes in a double pipe heat exchanger. J Ther Eng 2019;5:293–301. [CrossRef]

[9] Tokgöz N, Aksoy MM, Şahin B. Experimental investigation of flow characteristics of corrugated channel flow using PIV. J Ther Eng 2016;2:754–760. [CrossRef]

[10] Alempour SM, Arani AAA, Najafizadeh MM. Numerical investigation of nanofluid flow characteristics and heat transfer inside a twisted tube with elliptic cross section. J Therm Anal Calorim 2020;140:1237−1257. [CrossRef]

[11] Ahmadi-Senichault A, Arani AAA, Lasseux D. Numerical simulation of two-phase inertial flow in heterogeneous porous media. Transp Porous Media 2010;84:177−200. [CrossRef]

[12] Arani AAA, Mahmoodi M, Mazrouei Sebdani S. On the cooling process of nanofluid in a square enclosure with linear temperature distribution on left wall. J Appl Fluid Mech 2014;7:591−601. [CrossRef]

[13] Arani AAA, Abbaszadeh M, Ardeshiri A. Mixed convection fluid flow and heat transfer and optimal distribution of discrete heat sources location in a cavity filled with nanofluid. Chall Nano Micro Scale Sci Technol 2017;5:30−43.

[14] Sadripour S, Chamkha AJ. The effect of nanoparticle morphology on heat transfer and entropy generation of supported nanofluids in a heat sink solar collector. Therm Sci Eng Prog 2019;9:266−280. [CrossRef]

[15] Khudheyer AF, Al-Abbas AH, Carutasiu MB, Necula H. Turbulent heat transfer for internal flow of ethylene Glycol-Al_2O_3 nanofluid in a spiral grooved tube with twisted tape inserts. J Ther Eng 2021;7:761–772. [CrossRef]

[16] Tokgöz N, Alıç E, Kaşka Ö, Aksoy MM. The numerical study of heat transfer enhancement using Al_2O_3-water nanofluid in corrugated duct application. J Ther Eng 2018;4:1984–1997. [CrossRef]

[17] Azeez K, Abu Talib AR, Ahmed RI. Heat transfer enhancement for corrugated facing step channels using aluminium nitride nanofluid - numerical investigation. J Ther Eng 2022;8:734–747. [CrossRef]

[18] Arani AAA, Kakoli E, Hajialigol N. Double-diffusive natural convection of Al_2O_3-water nanofluid in an enclosure with partially active side walls using variable properties. J Mech Sci Technol 2015;28:4681−4691. [CrossRef]

[19] Arani AAA, Pourmoghadam F. Experimental investigation of thermal conductivity behavior of MWCNTS-Al_2O_3/ethylene glycol hybrid Nanofluid: providing new thermal conductivity correlation. Heat Mass Transf 2019;55:2329−2339. [CrossRef]

[20] Ehteram HR, Arani AAA, Sheikhzadeh GA, Aghaei A, Malihi AR. The effect of various conductivity and viscosity models considering Brownian motion on nanofluids mixed convection flow and heat transfer. Chall Nano Micro Scale Sci Technol 2016;4:19−28.

[21] Esfe MH, Arani AAA, Aghaie A, Wongwises S. Mixed convection flow and heat transfer in an up-driven, inclined, square enclosure subjected to DWCNT-water nanofluid containing three circular heat sources. Curr Nanosci 2017;13:311−323. [CrossRef]

[22] Zainal NA, Nazar R, Naganthran K, Pop I. MHD mixed convection stagnation point flow of a hybrid nanofluid past a vertical flat plate with convective boundary condition. Chin J Phys 2020;66:630−644. [CrossRef]

[23] Mahmoodi M, Arani AAA, Mazrouei S, Nazari S, Akbari M. Free convection of a nanofluid in a square cavity with a heat source on the bottom wall and partially cooled from sides. Therm Sci 2014;18:283−300. [CrossRef]

[24] Arani AAA, Ababaei A, Sheikhzadeh GA, Aghaei A. Numerical simulation of double-diffusive mixed convection in an enclosure filled with nanofluid using Bejan's heatlines and masslines. Alex Eng J 2018;57:1287−1300. [CrossRef]

[25] Lyu Z, Pourfattah F, Arani AAA, Asadi A, Foong LK. On the thermal performance of a fractal microchannel subjected to water and kerosene carbon nanotube nanofluid. Sci Rep 2020;10:7243. [CrossRef]
[26] Arani AAA, Amani J, Esfeh MH. Numerical simulation of mixed convection flows in a square double lid-driven cavity partially heated using nanofluid. J Nanostr 2012;2:301−311.
[27] Job VM, Gunakala SR. Numerical study of pulsatile MHD counter-current nanofluid flows through two elastic coaxial pipes containing porous blocks. Int J Heat Mass Transf 2017;113:1265−1280. [CrossRef]
[28] Garmroodi MRD, Ahmadpour A, Talati F. MHD mixed convection of nanofluids in the presence of multiple rotating cylinders in different configurations: A two-phase numerical study. Int J Mech Sci 2019;150:247−264. [CrossRef]
[29] Eid MR. Chemical reaction effect on MHD boundary-layer flow of two-phase nanofluid model over an exponentially stretching sheet with a heat generation. J Mol Liq 2016;220:718−725. [CrossRef]
[30] Ma Y, Mohebbi R, Rashidi MM, Yang Z. MHD convective heat transfer of Ag-MgO/water hybrid nanofluid in a channel with active heaters and coolers. Int J Heat Mass Transf 2019;137:714−726. [CrossRef]
[31] Sheikholeslami M, Rokni HB. Influence of melting surface on MHD nanofluid flow by means of two phase model. Chin J Phys 2017;55:1352−1360. [CrossRef]
[32] Jafarimoghaddam A. Two-phase modeling of three-dimensional MHD porous flow of Upper-Convected Maxwell (UCM) nanofluids due to a bidirectional stretching surface: Homotopy perturbation method and highly nonlinear system of coupled equations. Eng Sci Technol Int J 2018;21:714−726. [CrossRef]
[33] Eid MR, Mahny KL. Unsteady MHD heat and mass transfer of a non-Newtonian nanofluid flow of a two-phase model over a permeable stretching wall with heat generation/absorption. Adv Powder Technol 2017;28:3063−3073. [CrossRef]
[34] Sajid MU, Ali H. Recent advances in application of nanofluids in heat transfer devices: A critical review. Renew Sust Energ Rev 2019;103:556−592. [CrossRef]
[35] Kumar V, Sarkar J. Experimental hydrothermal behavior of hybrid nanofluid for various particle ratios and comparison with other fluids in minichannel heat sink. Int Commun Heat Mass Transf 2020;110:104397. [CrossRef]
[36] Izadi A, Siavashi M, Rasam H, Xiong Q. MHD enhanced nanofluid mediated heat transfer in porous metal for CPU cooling. Appl Therm Eng 2019;168:114843. [CrossRef]
[37] Sheikholeslami M. CuO-water nanofluid flow due to magnetic field inside a porous media considering Brownian motion. J Mol Liq 2018;249:921−929. [CrossRef]
[38] Soudagar MEM, Kalam MA, Sajid MU, Afzal A, Banapurmath NR, Akram N, et al. Thermal analyses of minichannels and use of mathematical and numerical models. Num Heat Transf Part A: Appl 2020;770:497−537. [CrossRef]
[39] Selimefendigil F, Öztop HF. MHD Pulsating forced convection of nanofluid over parallel plates with blocks in a channel. Int J Mech Sci 2019;157−158:726-740. [CrossRef]
[40] Shirazi M, Shateri A, Bayareh M. Numerical investigation of mixed convection heat transfer of a nanofluid in a circular enclosure with a rotating inner cylinder. J Therm Anal Calorim 2018;133:1061−1073. [CrossRef]
[41] Sepyani M, Shateri A, Bayareh M. Investigating the mixed convection heat transfer of a nanofluid in a square chamber with a rotating blade. J Therm Anal Calorim 2019;135:609−623. [CrossRef]
[42] Bayareh M, Kianfar A, Kasaeipoor A. Mixed convection heat transfer of water-alumina nanofluid in an inclined and baffled C-Shaped enclosure. J Heat Mass Transf Res 2018;5:129−138.
[43] Bayareh M, Nourbakhsh A, Khadivar ME. Numerical simulation of heat transfer over a flat plate with a triangular vortex generator. Int J Heat Technol 2018;36:1493−1501. [CrossRef]
[44] Vanaki SM, Mohammed HA, Abdollahi A, Wahid MA. Effect of nanoparticle shapes on the heat transfer enhancement in a wavy channel with different phase shifts. J Mol Liq 2014;196:32−42. [CrossRef]
[45] ANSYS Inc. Ansys Fluent-solver Theory Guide, 2009. Available at: https://www.afs.enea.it/project/neptunius/docs/fluent/html/th/node1.htm. Accessed Nov 9, 2023.
[46] Behzadmehr A, Saffar-Avval M, Galanis N. Prediction of turbulent forced convection of a nanofluid in a tube with uniform heat flux using a two phase approach. Int J Heat Fluid Flow 2007;28:211−219. [CrossRef]
[47] Hejazian M, Moraveji MK, Beheshti A. Comparative study of Euler and mixture models for turbulent flow of Al_2O_3 nanofluid inside a horizontal tube. Int Commun Heat Mass Transf 2014;52:152−158. [CrossRef]
[48] Goktepe S, Atalık K, Erturk H. Comparison of single and two-phase models for nanofluid convection at the entrance of a uniformly heated tube. Int J Ther Sci 2014;80:83−93. [CrossRef]
[49] Vyas A, Mishra B, Srivastava A. Investigation of the effect of blockage ratio on flow and heat transfer in the wake region of a cylinder embedded in a channel using whole field dynamic measurements. Int J Ther Sci 2020;153:106322. [CrossRef]
[50] Kim D, Kwon Y, Cho Y, Li C, Cheong S, Hwang Y, et al. Convective heat transfer characteristics of nanofluids under laminar and turbulent flow conditions. Curr Appl Phys 2009;9:119−123. [CrossRef]

[51] Patankar SV. Numerical heat transfer and fluid flow. 1980. Available at: https://catatanstudi.files.wordpress.com/2010/02/numerical-heat-transfer-and-fluid-flow.pdf. Accessed Nov 9, 2023.
[52] Tzirtzilakis EE, Xenos MA, Loukopoulos VC, Kafoussias N. Turbulent biomagnetic fluid flow in a rectangular channel under the action of a localized magnetic field. Int J Eng Sci 2006;44:1205−1224. [CrossRef]
[53] Tzirtzilakis EE, Sakalis VD, Kafoussias NG, Hatzikonstantinou PM. Biomagnetic fluid flow in a 3D rectangular duct. Int J Num Math Fluids 2004;44:1279−1298. [CrossRef]
[54] Aminfar H, Mohammadpourfard M, Kahnamouei YN. A 3D numerical simulation of mixed convection of a magnetic nanofluid in the presence of non-uniform magnetic field in a vertical tube using two phase mixture model. J Magn Magn Mater 2011;323:1963−1972. [CrossRef]
[55] Suman S, Khan MK, Pathak M. Performance enhancement of solar collectors - a review. Renew Sust Energ Rev 2015;49:192−210. [CrossRef]
[56] Sundar LS, Naik MT, Sharma KV, Singh MK, Reddy TCS. Experimental investigation of forced convection heat transfer and friction factor in a tube with Fe_3O_4 magnetic nanofluid. Exp Therm Fluid Sci 2012;37:65−71. [CrossRef]
[57] He YL, Xiao J, Cheng ZD, Tao YB. A MCRT and FVM coupled simulation method for energy conversion process in parabolic trough solar collector. Renew Energ 2011;36:976−985. [CrossRef]
[58] Sadaghiyani OK, Pesteei SM, Mirzaee I. Numerical study on heat transfer enhancement and friction factor of LS-2 parabolic solar collector. J Therm Sci Eng Appl 2013;6:12001−12010. [CrossRef]
[59] Cheng ZD, He YL, Xiao J, Tao YB, Xu RJ. Three-dimensional numerical study of heat transfer characteristics in the receiver tube of parabolic trough solar collector. Int Commun Heat Mass Transf 2010;37:782−787. [CrossRef]
[60] Cheng ZD, He YL, Cui FQ, Xu RJ, Tao YB. Numerical simulation of a parabolic trough solar collector with non-uniform solar flux conditions by coupling FVM and MCRT method. Sol Energ 2012;86:1770−1784. [CrossRef]
[61] Sokhansefat T, Kasaeian A, Kowsary F. Heat transfer enhancement in parabolic trough collector tube using Al2O3/synthetic oil nanofluid. Renew Sust Energ Rev 2014;33:636−644. [CrossRef]
[62] Molana M, Dogonchi AS, Armaghani T, Chamkha AJ, Ganji DD, Tlili I. Investigation of hydrothermal behavior of Fe_3O_4-H_2O nanofluid natural convection in a novel shape of porous cavity subjected to Magnetic Field Dependent (MFD) viscosity. J Energy Storage 2020;30:101395. [CrossRef]
[63] Sha L, Ju Y, Zhang H, Wang J. Experimental investigation on the convective heat transfer of Fe_3O_4/water nanofluids under constant magnetic field. Appl Therm Eng 2017;113:566−574. [CrossRef]
[64] Timofeeva EV, Routbort JL, Singh D. Particle shape effects on thermophysical properties of alumina nanofluids. J Appl Phys 2009;106:014304. [CrossRef]
[65] Dogonchi AS, Asghar Z, Waqas M. CVFEM simulation for Fe_3O_4-H_2O nanofluid in an annulus between two triangular enclosures subjected to magnetic field and thermal radiation. Int Commun Heat Mass Transf 2020;112:104449. [CrossRef]